Atmos. Meas. Tech., 9, 1833–1843, 2016
www.atmos-meas-tech.net/9/1833/2016/
doi:10.5194/amt-9-1833-2016

Atmospheric Measurement Techniques
Open Access
EGU

Measuring the morphology and density of internally mixed black carbon with SP2 and VTDMA: new insight into the absorption enhancement of black carbon in the atmosphere

Yuxuan Zhang[1], Qiang Zhang[1,6], Yafang Cheng[2], Hang Su[2], Simonas Kecorius[3], Zhibin Wang[3,2], Zhijun Wu[4,3], Min Hu[4,6], Tong Zhu[4,6], Alfred Wiedensohler[3], and Kebin He[5,6]

[1]Ministry of Education Key Laboratory for Earth System Modeling, Center for Earth System Science, Tsinghua University, Beijing 100084, China
[2]Multiphase Chemistry Department, Max Planck Institute for Chemistry, 55020 Mainz, Germany
[3]Leibniz-Institute for Tropospheric Research, 04318 Leipzig, Germany
[4]State Key Joint Laboratory of Environmental Simulation and Pollution Control, College of Environmental Sciences and Engineering, Peking University, Beijing 100871, China
[5]State Key Joint Laboratory of Environment Simulation and Pollution Control, School of Environment, Tsinghua University, Beijing 100084, China
[6]The Collaborative Innovation Center for Regional Environmental Quality, Beijing 100084, China

Correspondence to: Qiang Zhang (qiangzhang@tsinghua.edu.cn) and Hang Su (h.su@mpic.de)

Received: 1 October 2015 – Published in Atmos. Meas. Tech. Discuss.: 18 November 2015
Revised: 15 March 2016 – Accepted: 19 April 2016 – Published: 27 April 2016

Abstract. The morphology and density of black carbon (BC) cores in internally mixed BC (In-BC) particles affect their mixing state and absorption enhancement. In this work, we developed a new method to measure the morphology and effective density of the BC cores of ambient In-BC particles using a single-particle soot photometer (SP2) and a volatility tandem differential mobility analyzer (VTDMA) during the CAREBeijing-2013 campaign from 8 to 27 July 2013 at Xianghe Observatory. This new measurement system can select size-resolved ambient In-BC particles and measure the mobility diameter and mass of the In-BC cores. The morphology and effective density of the ambient In-BC cores are then calculated. For the In-BC cores in the atmosphere, changes in their dynamic shape factor (χ) and effective density (ρ_{eff}) can be characterized as a function of the aging process ($D_{\mathrm{p}}/D_{\mathrm{c}}$) measured by SP2 and VTDMA. During an intensive field study, the ambient In-BC cores had an average shape factor χ of $\sim$1.2 and an average density of $\sim 1.2\,\mathrm{g\,cm^{-3}}$, indicating that ambient In-BC cores have a near-spherical shape with an internal void of $\sim$30 %. From the measured morphology and density, the average shell / core ratio and absorption enhancement (E_{ab}) of ambient BC were estimated to be 2.1–2.7 and 1.6–1.9, respectively, for In-BC particles with sizes of 200–350 nm. When the In-BC cores were assumed to have a void-free BC sphere with a density of $1.8\,\mathrm{g\,cm^{-3}}$, the shell / core ratio and E_{ab} were overestimated by $\sim$13 and $\sim$17 %, respectively. The new approach developed in this work improves the calculations of the mixing state and optical properties of ambient In-BC particles by quantifying the changes in the morphology and density of ambient In-BC cores during aging.

1 Introduction

The light-absorbing capabilities of black carbon (BC)-containing particles are closely related to their morphology and density in the atmosphere (Zhang et al., 2008; Rissler et al., 2014), which are affected by their aging processes (Rissler et al., 2013; Geller et al., 2006). Fresh or externally mixed BC (Ex-BC) particles near emissions sources exist in fractal-like agglomerates, consisting of small carbon spherules with sizes of 15–30 nm that formed via coagulation processes (Park et al., 2003; Slowik et al., 2004;

Petzold et al., 2013). The physicochemical characteristics of BC-containing particles undergo significant changes during the aging process in the atmosphere, forming an internally mixed BC (In-BC) particle consisting of a BC core and coating materials (Cheng et al., 2006). When coated with a non-absorbing shell, void-containing BC particles with open structures transform into compact BC cores with near-spherical morphologies, fewer internal voids and higher densities, thereby decreasing the core size and increasing the BC core's refractive index (Bond and Bergstrom, 2006; Qiu et al., 2012; Khalizov et al., 2013). According to Mie theory, the absorption enhancement of In-BC depends on its BC core size, coating thickness and the refractive indexes of both the BC core and the coating (Fuller et al., 1999; Bond et al., 2006; Lack and Cappa, 2010). Thus, understanding the atmospheric evolution of the morphology and density of the BC core is important for investigating the optical properties of In-BC particles because the size and refractive index of the BC core are determined by its morphology and density (Adler et al., 2010; Scarnato et al., 2013; Radney et al., 2014).

To date, the absorption enhancement of In-BC particles is still unclear, partly because of a lack of understanding regarding the evolution of the morphology and density of BC-containing particles in the atmosphere (Xue et al., 2009a; Knox et al., 2009; Chan et al., 2011; Cappa et al., 2012). Recent in situ measurements have indicated that the absorption enhancement of In-BC particles may have been overestimated previously (Cappa et al., 2012) because the In-BC core was treated as a void-free sphere throughout its atmospheric lifetime when calculating the absorption enhancement of In-BC particles (Jacobson, 2000, 2001; Bond et al., 2006). This improper assumption may have led to significant bias in the absorption enhancement estimates by omitting the evolution of the morphology and density of the BC core during atmospheric aging and ignoring the impact of the aging time on the absorption enhancement.

To quantify how the morphology and density changes of the BC cores affect the absorption enhancement of ambient In-BC particles, an online measurement system able to separate Ex-BC and In-BC particles is needed because those Ex-BC fractions can induce unpredictable errors when calculating the morphology of In-BC cores. The morphology of aerosol particles can be measured using several measurement techniques, including transmission electron microscopy, angular light scattering, atomic force microscopy, differential mobility analyzer-electrical low-pressure impactors and differential mobility analyzer-aerosol particle mass analyzers (DMA-APMs) (Köylü et al., 1995; Sgro et al., 2003; Maricq and Ning, 2004; McMurry et al., 2002). However, none of these techniques can distinguish between the Ex-BC and In-BC cores in the atmosphere. Changes in the core morphologies and densities of In-BC particles are usually assessed experimentally using lab-generated BC cores and by mimicking the formation of In-BC particles during atmospheric aging (e.g., Qiu et al., 2012). For example, DMA-APM in combination with a heating unit can remove the coating materials from BC-containing particles and estimate the morphology and density of the BC component by determining the mobility diameter and particle mass of the BC core (Zhang et al., 2008; Pagels et al., 2009). Because DMA-APM cannot isolate the influence of Ex-BC particles, it is used only in laboratory measurements with generated Ex-BC or In-BC particles (McMurry et al., 2002; Xue et al., 2009b).

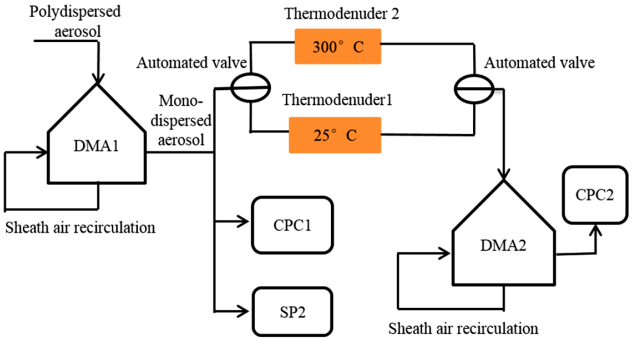

Figure 1. Schematic of the instrument setup.

In this study, we develop a novel method for in situ measurements of the morphology and effective density of ambient In-BC cores using a volatility tandem differential mobility analyzer (VTDMA) and a single-particle soot photometer (SP2). This combined VTDMA-SP2 system provides direct measurements of the mobility diameter and single-particle mass of the In-BC cores, which are then used to determine their morphology and effective density. The evolution of the morphology and density of the ambient In-BC cores during the aging process are characterized using this new approach. Finally, the absorption enhancement of the ambient In-BC aerosols is estimated by considering the core morphology and density.

2 Methods and data

2.1 Measurement system

A new measurement system is developed to obtain the morphology, density, mixing state and optical properties of ambient In-BC particles, as shown in Fig. 1. This system consists of a VTDMA (Leibniz Institute for Tropospheric Research, Leipzig, Germany) and an SP2 (Droplet Measurement Technologies, Boulder, CO, USA). Ambient aerosols were collected using a sampling system comprising a PM_{10} cyclone inlet and a silica-gel diffusion dryer system (Tuch et al., 2009).

The VTDMA section, which includes two differential mobility analyzers (DMAs), two condensation particle counters (CPCs) and two thermodenuders, is used to determine the mobility diameter (D_m) of the In-BC cores. The VTDMA investigates the mixing state of BC particles by measuring

how the aerosol particle size changes as the temperature is varied. The specifications for the VTDMA have been previously reported in the literature (Philippin et al., 2004; Wehner et al., 2009; Cheng et al., 2012). Briefly, quasi-monodisperse particles with sizes of 200, 250, 300 and 350 nm are preselected using the first DMA (DMA1) and counted with the first CPC (CPC1). These particles then pass through a thermodenuder at 300 °C (or 25 °C for the control group). BC, as a refractory component, remains in the particle phase after heating, whereas the other components tend to evaporate, thereby altering the particle size (Cheng et al., 2009). Therefore, the Ex-BC size exhibits little to no change, but the In-BC size will significantly decrease because of the evaporation of the coatings. This change is then measured using the second DMA (DMA2) and CPC (CPC2) to differentiate between the In-BC and the Ex-BC and to derive the D_{m} of the In-BC cores.

As shown in Fig. 1, the SP2 instrument also measures the mobility diameter-selected ambient particles to obtain the particle-to-particle mass of the refractory BC (rBC) and the scattering cross section of the In-BC particles. In the SP2 technique, the rBC mass in a single particle is determined from its laser-induced incandescence. The SP2 uses a continuous Nd:YAG intra-cavity laser beam at 1064 nm to heat a BC-containing particle to its vaporization temperature of $\sim$ 4000 K (Schwarz et al., 2006), at which point, detectable amounts of thermal radiation ("incandescent light") are emitted. The intensity of the thermal radiation is linearly proportional to the rBC mass (Moteki and Kondo, 2010; Baumgardner et al., 2012). The SP2 must be accurately calibrated to measure the effective density of the BC particles using the DMA-SP2 system, which requires knowledge of the mobility-diameter–mass relationship (i.e., the effective density) of the BC particles used for calibration (Gysel et al., 2011). In our study, we used Aquadag with size-resolved effective densities for the calibration. The calibration curve was fitted by recording the incandescence signal peak heights for Aquadag particles of known masses.

The SP2 technique also characterizes the scattering cross sections of individual In-BC particles based on their scattering signals. The scattering signal is calibrated using polystyrene latex spheres. Retrieving the scattering cross section data is very challenging because the initial scattering properties change as the coatings of the BC-containing particles evaporate. To overcome this problem, Gao et al. (2007) developed a leading edge only (LEO) fit method to derive the initial scattering properties of BC-containing particles. The validity of the LEO fit used for ambient BC-free and BC-containing particles is investigated here (see Fig. S1 in the Supplement). In addition, the SP2 measurements separate the In-BC and Ex-BC particles based on the delay times of the peaks between the incandescence and scattering signals. In our study, a delay time of 1.6 µs was chosen to discriminate between Ex-BC ($<$ 1.6 µs) and In-BC ($\geq$ 1.6 µs) types according to the delay time distribution obtained from the SP2 measurements (Fig. S2).

The measurement system was deployed at the Xianghe Atmospheric Observatory (39.80° N, 116.96° E) from 8 to 27 July 2013, as part of the CAREBeijing-2013 campaign. The Xianghe site is located in the southeast region of Beijing ($\sim$ 60 km) and the northwest region of the megacity Tianjin ($\sim$ 100 km). Xianghe is a polluted regional background site influenced by mixed regional emission sources from the Jing–Jin–Ji region. The Xianghe Observatory is surrounded by residential areas and is located approximately 5 km from the local town center.

2.2 Theoretical calculation

2.2.1 Morphology and effective density

In this study, the morphology of In-BC cores is characterized by the particle size, shape factor (χ) and void ratio (R_{void}) (DeCarlo et al., 2004). Ambient aerosols are usually non-spherical particles (e.g., BC aggregates), and as such, their structural parameters are complex. The size of irregular particles is determined as an equivalent diameter, i.e., mobility diameter (D_{m}) (Khalizov et al., 2013). Meanwhile, the density of the BC cores is characterized by the effective density (ρ_{eff}) (Zhang et al., 2008). These parameters can be calculated as described below.

The ρ_{eff} of the In-BC core is calculated as the mass (m, fg)-to-D_{m} ratio based on the SP2 and VTDMA measurements, respectively, assuming that the In-BC core is a sphere. Then, ρ_{eff} can be written as

$$\rho_{\mathrm{eff}} = \frac{6m}{\pi D_{\mathrm{m}}^3}. \tag{1}$$

The χ of the In-BC core is calculated from D_{m} and the mass-equivalent diameter (D_{me}) using Eq. (2).

$$\chi = \frac{D_{\mathrm{m}} \times C_{\mathrm{c}}(D_{\mathrm{me}})}{D_{\mathrm{me}} \times C_{\mathrm{c}}(D_{\mathrm{m}})} \tag{2}$$

In Eq. (2), D_{me} is calculated from the mass of the rBC measured using SP2 by assuming a density of 1.8 g cm^{-3}, and C_{c} is the Cunningham slip correction factor, parameterized as

$$C_{\mathrm{c}}(D) = 1 + \frac{2\lambda}{D}\left[\alpha + \beta \exp\left(-\frac{\gamma \times D}{2\lambda}\right)\right], \tag{3}$$

where D is the particle size (D_{me} or D_{m}), and λ is the mean free path of the gas molecules (65 nm in our study); the empirical constants α, β and γ are 1.142, 0.558 and 0.999, respectively (Allen and Raabe, 1985).

Assuming a spherical core in the In-BC particle, R_{void} is calculated using the D_{me} and D_{m} of the In-BC core with Eq. (4).

$$R_{\mathrm{void}} = 1 - \frac{D_{\mathrm{me}}^3}{D_{\mathrm{m}}^3} \tag{4}$$

2.2.2 Absorption enhancement

The absorption enhancement (E_{ab}) of the In-BC particles is defined as the ratio of the absorption cross sections of the coated BC particles ($C_{ab,p}$) and the bare BC cores ($C_{ab,c}$), which are calculated according to the core size (D_c), the particle size (D_p) and the refractive indices of the non-BC coatings (RI_{nonBC}) and the BC cores (RI_c) using the Mie model at a wavelength of 550 nm, as given in Eq. (5):

$$E_{ab} = \frac{C_{ab,p}(D_c,\ D_p,\ RI_{nonBC},\ RI_c)}{C_{ab,c}(D_c,\ RI_c)}, \quad (5)$$

where D_c is derived from the mass (m) of the rBC measured by SP2 and its density (ρ_c). Previously, a prescribed ρ_c value of 1.8 g cm^{-3} was used, assuming a void-free spherical core in the In-BC particle (Moteki and Kondo, 2010; Cappa et al., 2012). In this work, the ρ_c is characterized by the effective density (ρ_{eff}), considering the morphology (χ and R_{void}) of the In-BC core. In summary, D_c is calculated by Eq. (6):

$$D_c = \left(\frac{6m}{\pi\rho_c}\right)^{1/3} = \left(\frac{6m}{\pi\rho_{eff}}\right)^{1/3}, \quad (6)$$

whereD_p is determined by the Mie theory calculation with a shell-and-core mode (Metcalf et al., 2013) relating to C_s, D_c and RI_{nonBC} and RI_c, as shown in Eq. (7):

$$D_p \sim (C_s, D_c RI_{nonBC} RI_c), \quad (7)$$

where C_s is obtained from the SP2 scattering signal using the LEO fit (Gao et al., 2007). The RI_{nonBC} used in this study is deduced from the SP2-VTDMA measurements and Mie theory calculations, as described in the supplemental information (Fig. S3). Given that voids in the In-BC cores can be filled by air, non-BC components or both, we selected two ideal cases to calculate the RI_c in the following analysis: all voids filled with air (RI_c(air)) and all voids filled by non-BC components (RI_c(nonBC)); these cases are described by Eqs. (8) and (9), respectively.

$$RI_c(\text{air}) = [n_{BC} \times (1 - R_{void}) + n_{air} \times R_{void}] + [k_{BC} \times (1 - R_{void})]i \quad (8)$$

$$RI_c(\text{nonBC}) = [n_{BC} \times (1 - R_{void}) + n_{nonBC} \times R_{void}] + [k_{BC} \times (1 - R_{void})]i \quad (9)$$

In Eqs. (8) and (9), n_{BC}, n_{air} and n_{nonBC} are the real parts of RI for the BC materials, air and non-BC components (with $n_{BC} = 1.95$, $n_{air} = 1.0$ and $n_{nonBC} = 1.42$), respectively, and k_{BC} is the imaginary part of the refractive index for BC ($k_{BC} = 0.79$) (Bond and Bergstrom, 2006).

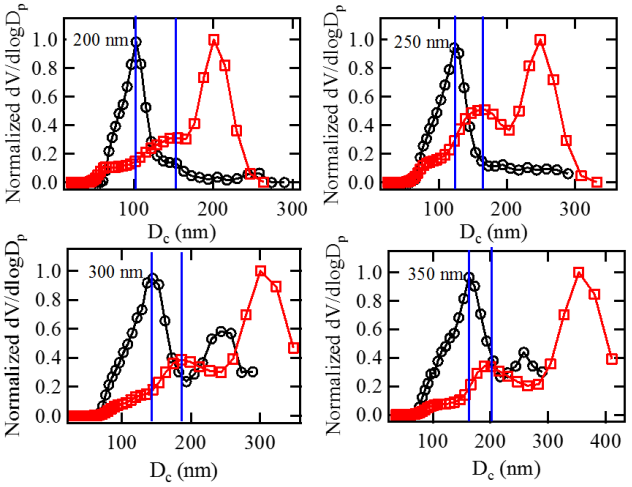

Figure 2. The normalized volume size distribution of the In-BC cores from the SP2 measurements (black marks and line) and the residual particles from the VTDMA measurements at 300 °C (red marks and line). Before the measurements were taken with SP2 at 300 °C, the initial particle sizes selected by DMA1 were 200, 250, 300 and 350 nm. The blue lines represent the In-BC core sizes at the peaks of the volume size distribution from the VTDMA and SP2 measurements. The In-BC core size is characterized by the mass-equivalent diameter determined from the SP2 measurement and the mobility diameter from the VTDMA measurement.

3 Results and discussion

3.1 Comparing the volume size distribution of In-BC cores measured by VTDMA and SP2

Figure 2 presents the volume size distributions of the mixed Ex-BC and In-BC cores measured by VTDMA and the In-BC cores measured by SP2 for the four prescribed size ranges through DMA1. After heating to 300 °C, the residual particles measured by VTDMA mainly include Ex-BC particles and In-BC cores (Philippin et al., 2004; Cheng et al., 2009). A bimodal distribution was observed in the VTDMA measurements, corresponding to the size distributions of the Ex-BC and In-BC cores. The peaks at the initially prescribed size ranges represent the Ex-BC particles, which did not undergo a size change after heating, and the peaks at smaller sizes represent the mobility diameters of the In-BC cores ($D_{c,m}$), which were 154–201 nm (Table 1) smaller than the initial mobility diameters with the coatings ($D_{p,m}$, 200–350 nm).

For the SP2 measurements presented in Fig. 2, the mass-equivalent size of an individual In-BC core ($D_{c,me}$) was calculated by the mass and density of the rBC (1.8 g cm^{-3}), assuming that the In-BC core has a void-free sphere morphology. The peaks in the SP2-measured size distributions of the In-BC cores were 102–161 nm (Table 1) smaller than their initial sizes, remarkably lower than the VTDMA measurements. The large discrepancy between the SP2 and VTDMA measurements suggests that the morphology of the In-

Table 1. The mobility diameter ($D_{c,m}$) and mass-equivalent diameter ($D_{c,me}$) of In-BC cores at peaks in the size distribution (Fig. 2) determined by VTDMA and SP2 of size-resolved In-BC particles of 200–350 nm ($D_{p,m}$).

$D_{p,m}$ (nm)	200	250	300	350
$D_{c,m}$ (nm)	154	165	190	201
$D_{c,me}$ (nm)	102	123	145	161

BC cores was not a void-free sphere because the inclusion of voids in In-BC cores results in lower density and larger size, as observed by VTDMA. In this case, the ρ_{BC} of 1.8 g cm^{-3} used to calculate the size of BC cores is inappropriate for the SP2 measurements.

3.2 Morphology and effective density of In-BC cores

3.2.1 The evolution with BC aging process

The differences in the sizes of the In-BC cores measured by SP2 and VTDMA were then used to derive the morphology and effective density of the In-BC cores. For each BC particle mobility diameter (200, 250, 300 and 350 nm) presented in Fig. 2, the peak in the SP2 measurements and the first peak in the VTDMA measurements represent the mass-equivalent diameter and the mobility diameter of the In-BC cores, respectively. Both the shape factor (χ) and the effective density (ρ_{eff}) of the In-BC cores were then calculated using Eqs. (1) and (2).

Figure 3 presents the evolution of χ and ρ_{eff} over the aging process recorded during the Xianghe campaign.The degree of aging for BC mixed with other species was quantified by the ratio between the coated BC particles (i.e., In-BC) and the bare BC-core sizes (D_p/D_c), which should significantly increase during the aging process because of the condensation of the coatings (Cappa et al., 2012). Changes in the core morphology and effective density strongly depend on the aging and can be quantified by measuring the size-resolved ambient In-BC particles with different aging degrees, as shown in Fig. 3. The shape factor of the In-BC cores decreased as the aging process proceeded and exhibited a power-law relationship (Fig. 3a), confirming that the In-BC core assumes a more regular shape as the coatings accumulate. The behavior of the measured In-BC cores during the atmospheric aging process suggests that their morphologies become more spherical with strong aging but still differ from the ideal sphere with a χ of 1. The effective density of the In-BC cores increased with the aging degree according to an exponential function (Fig. 3b), indicating that the In-BC cores become more compact during aging. The effective densities of the In-BC cores observed in this work were significantly lower than that of a void-free spherical BC core (1.8 g cm^{-3}), indicating that the In-BC cores exist as void-containing structures in the atmosphere. For the In-BC cores observed during the campaign,

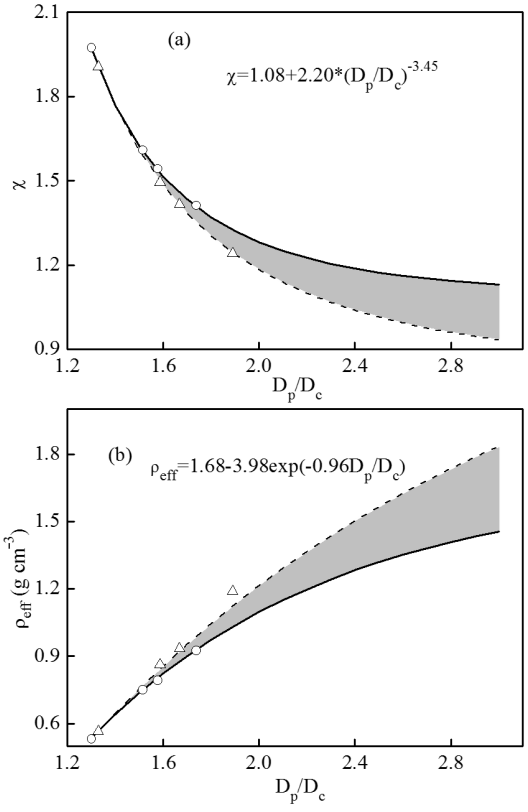

Figure 3. Changes in χ **(a)** and ρ_{eff} **(b)** of In-BC cores undergoing aging. The solid lines are fitted based on the data (circle markers) calculated by the measured peak values for size-resolved In-BC particles shown in Fig. 2; the dashed lines are fitted based on the data (triangle markers) derived from a 5 % non-volatile coating fraction; the grey shaded area represents the uncertainty in the morphology and density of the In-BC cores obtained here.

the average values of χ and ρ_{eff} were 1.2 and 1.2 g cm^{-3}, respectively, indicating that the In-BC cores sampled had near-spherical shapes with internal voids. Based on Eq. (4), the average fraction of internal voids was ∼ 30 %. In this case, the previously used assumption of a void-free sphere may have misrepresented the morphology and density of the In-BC cores in the atmosphere and introduced significant uncertainties in the estimated optical properties of the In-BC particles.

3.2.2 The uncertainties

It should be noted that the presence of a non-refractory component after the thermodenuder step (a part of VTDMA) can introduce biases in the measured mobility diameters of the In-BC cores. For example, the incomplete removal of the coatings will lead to an overestimation of the mobility diameter, resulting in the overestimation of χ and underestimation of ρ_{eff}. The removal of the non-refractory component from ambient BC-free and BC-containing particles using a

Table 2. Comparison of our method applied to atmospheric measurements and previous techniques used in laboratory measurements for determining the morphology and density of In-BC cores.

Methods	Mass measurement	Core	Coatings	D_{m} (nm)	D_{ve} (nm)	χ	ρ_{eff} (g cm^{-3})	Reference
VTDMA-SP2	SP2	rBC	Non-BC	150–200	100–160	1.4–2.0	0.5–0.9	This study
VTDMA-APM	APM	Soot	Sulfuric acid (1.4×10^{10} cm^{-3})	150–210		1.7–1.9	0.5–0.7	Pagels et al. (2009)
VTDMA-APM	APM	Soot	Sulfuric acid (2.5×10^{9} cm^{-3})	150–210			0.2–0.5	Pagels et al. (2009)
VTDMA-APM	APM	Soot	Succinic acid	150–200		2.4–3.0	0.2–0.4	Xue et al. (2009b)
VTDMA-APM	APM	Soot	Glutaric acid	150–240		1.8–2.0	0.6–1.0	Xue et al. (2009b)
VTDMA-AMS	AMS	Soot	Oleic acid		120–160	1.3–2.5		Slowik et al. (2007)
VTDMA-AMS	AMS	Soot	Anthracene	135–225	120–180	1.2–1.5		Slowik et al. (2007)

thermodenuder at 300 °C was determined by SP2 (Fig. S4). Generally, the first peak position of the volume size distribution of residual particles from the VTDMA measurements (Fig. 2 red lines) was dominated by In-BC cores and residual coatings, and the residual BC-free particles exerted little influence. The efficiency of the coating removal by the thermodenuder in our study was approximately 95 % (volume fraction).

Figure 3 also presents the relationships between χ, ρ_{eff} and the $D_{\mathrm{p}}/D_{\mathrm{c}}$ ratio, considering the effect of residual coatings on the volume size distribution in the VTDMA measurement. The presence of ~ 5 % residual coatings was found to lead to ~ 10 % uncertainty when using average values of χ (~ 1.2) and ρ_{eff} (1.2 g cm^{-3}). In addition, the uncertainties increased with the aging process because of the increasing accumulation of non-volatile coatings, indicating that the presence of residual coatings mainly influenced the calculation of the χ and ρ_{eff} of the In-BC cores with smaller sizes. However, the relationships between χ, ρ_{eff} and $D_{\mathrm{p}}/D_{\mathrm{c}}$ remained valid.

In contrast, the changes in the morphologies of the In-BC cores caused by the evaporation of the coating during heating can also lead to bias in the measured mobility diameter based on the VTDMA measurement. If the In-BC cores become less compact because of the evaporation of coatings during heating, the mobility diameter of the In-BC cores determined with DMA2 will be overestimated, leading to the overestimation of χ and underestimation of ρ_{eff}.

3.2.3 Comparison with previous laboratory studies

Laboratory measurements are widely used to determine the morphology and density of In-BC cores. In-BC particles are generated when flame soot particles are exposed to vapor (e.g., sulfuric acid), and the coatings are subsequently vaporized using a thermodenuder (e.g., 200 °C) to obtain bare In-BC cores. The morphology and density of the In-BC cores are then derived by measuring the particle mass and mobility diameter. The main difference between this work and previous reference techniques lies in the measurements of the mass of the In-BC cores (SP2 in this work vs. APM or aerosol mass spectrometer (AMS) previously).

Here, we compare our results with the laboratory measurements reported in the literature (Table 2). For the In-BC cores with D_{m} of 150–200 nm and D_{me} of 100–160 nm studied here, the observed χ and ρ_{eff} ranged from 1.4–2.0 and 0.5–0.9 g cm^{-3}, respectively. These ranges were generally in good agreement with the previously reported ranges of In-BC cores determined experimentally, indicating that the values of χ and ρ_{eff} observed in our study were reasonable. Therefore, our measurement method is valid for the determination of the morphology and density of In-BC cores.

3.3 Effects of In-BC core density on measurements of optical properties

3.3.1 Mixing state

Figure 4 presents the number size distribution of size-resolved In-BC particles calculated using the Mie model under different assumptions regarding the In-BC core densities. After selection by DMA1, the particles exhibited a polydispersed multimodal size distribution. The first peak represents the singly charged particles, in good agreement with the DMA1-prescribed size (200, 250, 300 or 350 nm). The second or third peak represents the distribution of multiply charged particles. To exclude the effects of multiply charged particles, we only selected the data populations that characterized singly charged particles near the first peak to investigate the shell / core ratios and absorption enhancement of In-BC particles.

As discussed in Sect. 2.2.2, the evolution of the core density of In-BC in the atmosphere could impact its absorption enhancement capability because the size and refractive indices of the BC core change during aging. Figure 5 presents the distribution of the shell / core ratio ($D_{\mathrm{p}}/D_{\mathrm{c}}$) of the size-resolved In-BC particles under different core density assumptions (1.0–1.8 g cm^{-3}) and void types (air or non-BC component). For all size ranges, higher shell / core ratios were observed as the In-BC core density increases, implying that In-BC cores become more compact during aging. The shell / core ratio increased by ~ 25 % when the In-BC core density increased from 1.0 to 1.8 g cm^{-3}. Compared to the average In-BC core density of 1.2 g cm^{-3} measured during

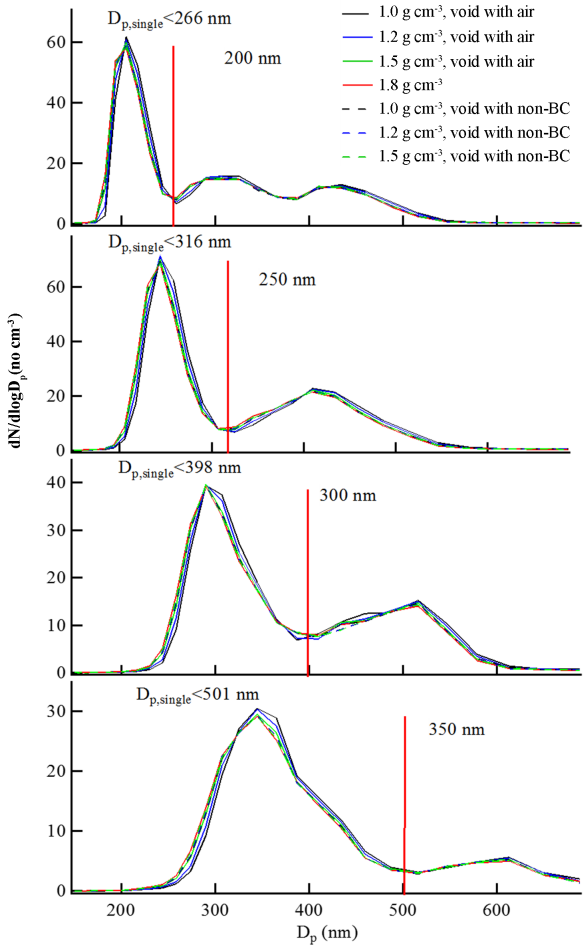

Figure 4. The number size distributions of size-resolved ambient In-BC particles with different core densities and void types.

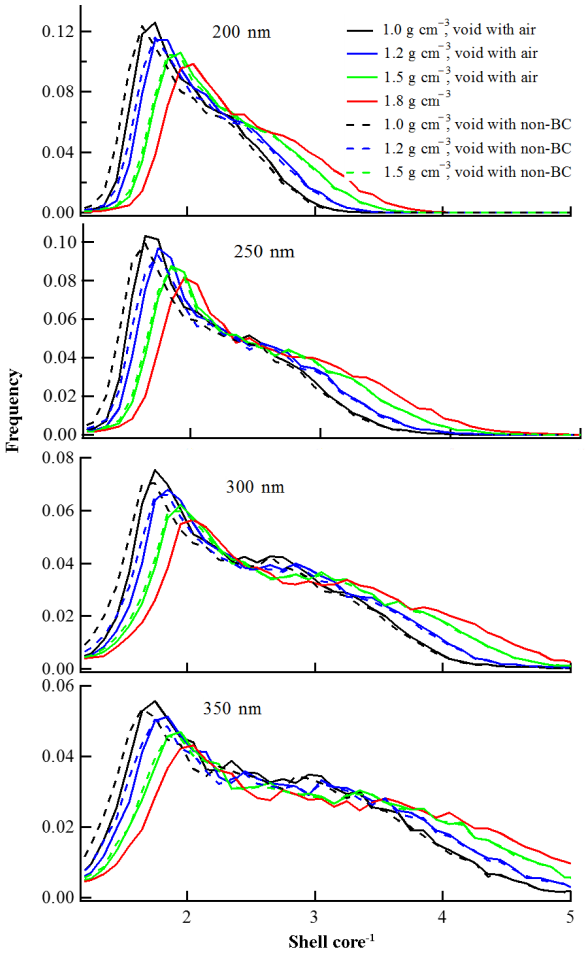

Figure 5. The shell / core ratios (D_p/D_c) of size-resolved ambient In-BC particles with different core densities and void types.

the campaign, the assumption that the In-BC core is a void-free sphere ($\rho = 1.8\,\mathrm{g\,cm^{-3}}$) could cause an overestimation of the shell / core ratio by as much as 13 %. This overestimation would, in turn, lead to an inaccurate assessment of the optical properties of ambient In-BC particles, as discussed in Sect. 3.3.2.

Throughout the campaign, the average shell / core ratio ranged between 2.1 and 2.7 for different particle size ranges. Larger particles tended to have higher shell / core ratios, indicating that the particle sizes and coating thicknesses increased during the aging process. The shell / core ratios were slightly larger for In-BC cores filled with air than for those filled with non-BC materials. For an individual In-BC particle with a given volume fraction of non-BC components measured by SP2, the existence of non-BC materials in the voids decreased the coating thickness, resulting in a lower shell / core ratio than that with an air-filled internal void.

3.3.2 Absorption enhancement

Figure 6 presents the light-absorption enhancement at 550 nm of size-resolved In-BC particles calculated by the Mie model for different core densities and void types. For the ambient In-BC particles with an average core density of $1.2\,\mathrm{g\,cm^{-3}}$ observed in Xianghe, the average light absorption was enhanced by 1.6–1.9 times by the atmospheric aging process. When the In-BC core was assumed to have a void-free spherical core with a density of $1.8\,\mathrm{g\,cm^{-3}}$, the Mie model would overestimate the light-absorption enhancement ratio by ~ 17 %. For polluted regions with large fractions of freshly emitted BC, the assumption that BC particles were void-free spheres would cause significant biases in light-absorption simulations. The new approach developed here estimates the absorption enhancement of ambient In-BC particles more accurately by considering the effects of the In-BC core morphology and density on light absorption. In the future, the simulation of the optical properties by the models could be improved by including the measured mor-

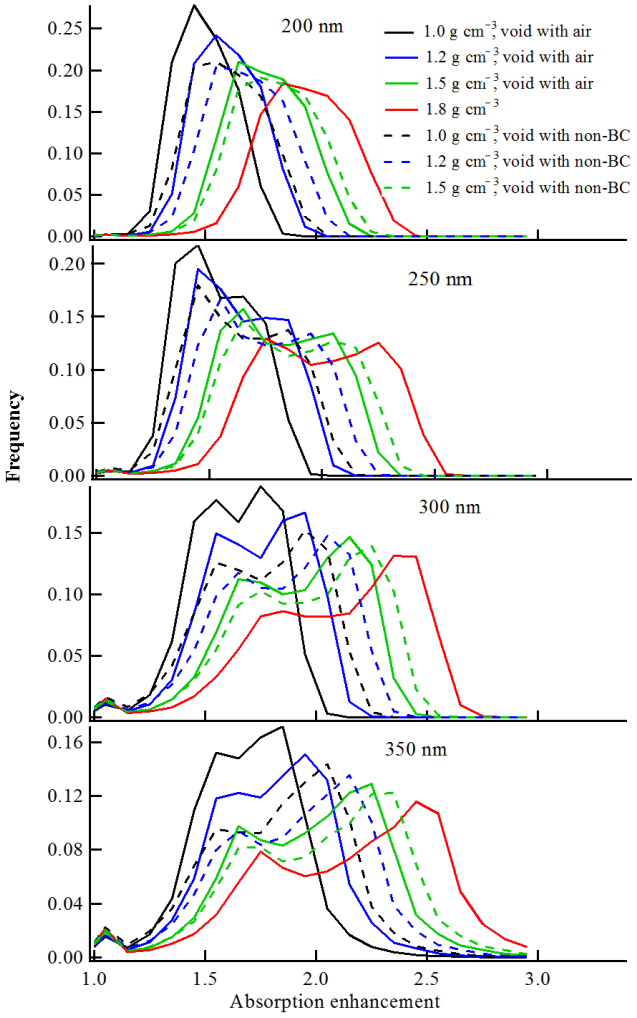

Figure 6. Absorption enhancement of size-resolved ambient In-BC particles with different core densities and void types.

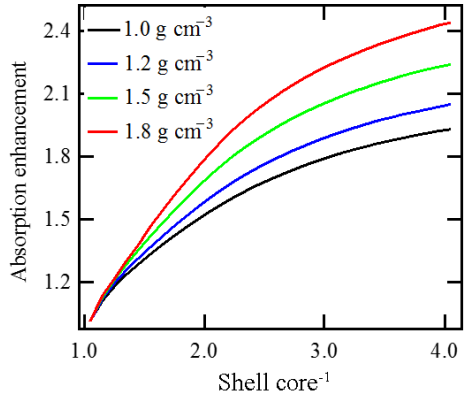

Figure 7. Changes in the absorption enhancement (E_{ab}) at 550 nm as the shell / core ratios (D_p/D_c) vary for size-resolved ambient In-BC particles (250 nm) with different core densities.

phologies and densities of In-BC cores when more in situ measurements for different regions are available.

Similar to the shell / core ratio, the absorption enhancement of In-BC particles increased with particle size because of the size growth of the BC particles, which primarily occurred via the condensation of non-BC components on the surface of the BC particles. The E_{ab} distribution showed one peak for In-BC particles at 200 nm but two peaks for particles at 250–350 nm, which were attributed to the various origins of the air mass at the Xianghe site. Smaller In-BC particles mainly have local origins and exhibit less light-absorption enhancement because of weaker aging, whereas the larger particles are delivered by regional transportation and have stronger aging, leading to stronger light-absorption enhancement. Moreover, the E_{ab} was greater for In-BC core voids filled with non-BC material than for air-filled ones, indicating that the existence of non-BC components in the core voids enhance BC absorption to a greater extent than the presence of these components on the surface of the BC core.

Figure 7 shows the changes in the absorption enhancement (E_{ab}) at 550 nm as the shell / core ratios (D_p/D_c) vary for size-resolved ambient In-BC particles (250 nm) with different core densities. The light-absorption enhancement (E_{ab}) of In-BC particles has been investigated based on the lensing effect theory (Fuller et al., 1999; Moffet et al., 2009; Lack and Cappa 2010), in which the coatings act as a lens and focus photons in the BC core. As shown in Fig. 7, the E_{ab} of the In-BC particles significantly increased as the shell / core ratio increased, confirming the coatings' lensing effect. Furthermore, significant increases in the E_{ab} as the core density increased at a given shell / core ratio provide strong evidence that the light absorption was enhanced by compact and dense BC cores. The contribution of the core density to the light-absorption enhancement could likely be attributed to the changes in the refractive index of the In-BC core (RI_c), as indicated by Eq. (8). Compared with the lensing effect, the relative contribution of the core density to the absorption enhancement was as high as ∼ 20 % as the core density increased from 1.0 to 1.8 g cm^{-3} for In-BC particles with a shell / core ratio of ∼ 3. The core density had an even greater contribution to the E_{ab} as the shell / core ratio increased among size-resolved In-BC particles, because the increase in E_{ab} caused by the lensing effect weaken as the coatings accumulate. In summary, the light-absorption enhancement of In-BC particles during the aging process is affected by both changes in the core density and the lensing effects.

4 Conclusions

The light-absorbing capability of In-BC aerosols depends on their morphology and density; however, the evolution of the morphology and density of BC cores in the atmosphere remain unknown. In this study, we designed a new measurement system by combining VTDMA and SP2 to measure

the morphology and density of ambient In-BC cores. In this new system, size-resolved ambient In-BC particles are initially selected using both VTDMA and SP2. The mobility diameter and mass of the In-BC cores are then measured by VTDMA and SP2, respectively, and these measurements are used to calculate the morphology and effective density of the In-BC cores. By considering the morphology and density of ambient In-BC cores, our work provides new insight into the enhancement of light absorption resulting from In-BC particles in the atmosphere.

Using our new system, we quantified the evolution of the morphology and density of ambient In-BC cores with aging during an intensive field campaign in North China in the summer of 2013. As the aging process progressed, the shape factor decreased and the effective density increased for the In-BC, indicating that the In-BC cores assumed more regular and compact shapes during aging. We found that very few In-BC cores became void-free spheres during the atmospheric aging process, and therefore, the effective density of most ambient In-BC cores was lower than the BC material density of $1.8\,\mathrm{g\,cm^{-3}}$. During the campaign period, the average shape factor and effective densities of the ambient In-BC cores were ~ 1.2 and $\sim 1.2\,\mathrm{g\,cm^{-3}}$, respectively, implying a near-spherical shape containing 30 % internal void in the ambient In-BC cores.

The light-absorption enhancement of the ambient In-BC particles was then calculated using the Mie model. The light-absorption enhancement ratio was estimated to be 1.6–1.9 based on the average In-BC core density ($1.2\,\mathrm{g\,cm^{-3}}$) observed in Xianghe, which was ~ 15 % lower than the values estimated assuming void-free spherical structures with densities of $1.8\,\mathrm{g\,cm^{-3}}$. We can then conclude that the previous models tend to overestimate the light absorption of BC particles over polluted regions where large fractions of BC are locally emitted.

Using the new measurement techniques developed here, the absorption enhancement of ambient BC particles can more accurately reflect the morphology and density of In-BC cores. To better understand the evolution of these parameters of In-BC cores during atmospheric aging, more in situ measurements in different regions should be conducted. In the future, the simulation of the optical properties of ambient BC-containing particles might be improved by characterizing the morphology and density of In-BC cores via in situ measurements.

The Supplement related to this article is available online at doi:10.5194/amt-9-1833-2016-supplement.

Acknowledgements. This study was supported by the National Natural Science Foundation of China (41222036, 21221004, 21190054, 41330635 and GZ 663) and the Environmental Protection Commonweal Project of China (201409027).

Edited by: P. Laj

References

Adler, G., Riziq, A. A., Erlick, C., and Rudich, Y.: Effect of Intrinsic Organic Carbon on the Optical Properties of Fresh Diesel Soot, P. Natl. Acad. Sci. USA, 107, 6699–6704, 2010.

Allen, M. D. and Raabe, O. G.: Slip Correction Measurements of Spherical Solid Aerosol-Particle s in an Improved Millikan Apparatus, Aerosol Sci. Tech., 4, 269–286, 1985.

Baumgardner, D., Popovicheva, O., Allan, J., Bernardoni, V., Cao, J., Cavalli, F., Cozic, J., Diapouli, E., Eleftheriadis, K., Genberg, P. J., Gonzalez, C., Gysel, M., John, A., Kirchstetter, T. W., Kuhlbusch, T. A. J., Laborde, M., Lack, D., Müller, T., Niessner, R., Petzold, A., Piazzalunga, A., Putaud, J. P., Schwarz, J., Sheridan, P., Subramanian, R., Swietlicki, E., Valli, G., Vecchi, R., and Viana, M.: Soot reference materials for instrument calibration and intercomparisons: a workshop summary with recommendations, Atmos. Meas. Tech., 5, 1869–1887, doi:10.5194/amt-5-1869-2012, 2012.

Bond, T. C. and Bergstrom R. W.: Light Absorption by Carbonaceous Particles: An Investigative Review, Aerosol Sci. Tech., 40, 27–67, 2006.

Bond, T. C., Habib, G., and Bergstrom, R. W.: Limitations in the enhancement of visible light absorption due to mixing state, J. Geophys. Res., 111, D20211, doi:10.1029/2006JD007315, 2006.

Cappa, C. D., Onasch, T. B., Massoli, P., Worsnop, D. R., Bates, T. S., Cross, E. S., Davidovits, P., Hakala, J., Hayden, K. L., Jobson, B. T., Kolesar, K. R., Lack, D. A., Lerner, B. M., Li, S. M., Mellon, D., Nuaaman, I., Olfert, J. S., Petaja, T., Quinn, P. K., Song, C., Subramanian, R., Williams, E. J., and Zaveri, R. A.: Radiative Absorption Enhancements Due to the Mixing State of Atmospheric Black Carbon, Science, 337, 1078–1081, 2012.

Chan, T. W., Brook, J. R., Smallwood, G. J., and Lu, G.: Time-resolved measurements of black carbon light absorption enhancement in urban and near-urban locations of southern Ontario, Canada, Atmos. Chem. Phys., 11, 10407–10432, doi:10.5194/acp-11-10407-2011, 2011.

Cheng, Y., Berghof, M., Garland, R. M., Wiedensohler, A., Wehner, B., Müller, T., Su, H., Zhang, Y., Achert, P., Nowak, A., Pöschl, U., Zhu, T., Hu, M., and Zeng, L.: Influence of soot mixing state on aerosol light absorption and single scattering albedo during air mass aging at a polluted regional site in northeastern China, J. Geophys. Res., 114, D010883, doi:10.1029/2008JD010883, 2009.

Cheng, Y. F., Eichler, H., Wiedensohler, A., Heintzenberg, J., Zhang, Y. H., Hu, M., Herrmann, H., Zeng, L. M., Liu, S., Gnauk, T., Brüggemann, E., and He, L. Y.: Mixing state of elemental carbon and non-light-absorbing aerosol components derived from in situ particle optical properties at Xinken in Pearl River Delta of China, J. Geophys. Res., 111, D20204, doi:10.1029/2005JD006929, 2006.

Cheng, Y. F., Su, H., Rose, D., Gunthe, S. S., Berghof, M., Wehner, B., Achtert, P., Nowak, A., Takegawa, N., Kondo, Y., Shiraiwa, M., Gong, Y. G., Shao, M., Hu, M., Zhu, T., Zhang,

Y. H., Carmichael, G. R., Wiedensohler, A., Andreae, M. O., and Pöschl, U.: Size-resolved measurement of the mixing state of soot in the megacity Beijing, China: diurnal cycle, aging and parameterization, Atmos. Chem. Phys., 12, 4477–4491, doi:10.5194/acp-12-4477-2012, 2012.

DeCarlo, P. F., Slowik, J. G., Worsnop, D. R., Davidovits, P., and Jimenez, J. L.: Particle morphology and density characterization by combined mobility and aerodynamic diameter measurements, Part 1: Theory, Aerosol Sci. Tech., 38, 1185–1205, 2004.

Fuller, K. A., Malm, W. C., and Kreidenweis, S. M.: Effects of mixing on extinction by carbonaceous particles, J. Geophys. Res., 104, 15941–15954, 1999.

Gao, R. S., Schwarz, J. P., Kelly, K. K., Fahey, D. W., Watts, L. A., Thompson, T. L., Spackman, J. R., Slowik, J. G., Cross, E. S., Han, J. H., Davidovits, P., Onasch, T. B., and Worsnop, D. R. A.: Novel Method for Estimating Light-Scattering Properties of Soot Aerosols Using a Modified Single-Particle Soot Photometer, Aerosol. Sci. Tech., 41, 125–135, 2007.

Geller, M., Biswas, S., and Sioutas, C.: Determination of particle effective density in urban environments with a differential mobility analyzer and aerosol particle mass analyzer, Aerosol Sci. Tech., 40, 709–723, 2006.

Gysel, M., Laborde, M., Olfert, J. S., Subramanian, R., and Gröhn, A. J.: Effective density of Aquadag and fullerene soot black carbon reference materials used for SP2 calibration, Atmos. Meas. Tech., 4, 2851–2858, doi:10.5194/amt-4-2851-2011, 2011.

Jacobson, M. Z.: A physically based treatment of elemental carbon optics: Implication for global direct forcing of aerosols, Geophys. Res. Lett., 27, 217–220, doi:10.1029/1999GL010968, 2000.

Jacobson, M. Z.: Strong radiative heating due to the mixing state of black carbon in atmospheric aerosol, Nature, 409, 695–697, 2001.

Khalizov, A. F., Lin, Y., Qiu, C., Guo, S., Collins, D., and Zhang R.: Role of OH-Initiated Oxidation of Isoprene in Aging of Combustion Soot, Environ. Sci. Technol., 47, 2254–2263, 2013.

Knox, A., Evans, G. J., Brook, J. R., Yao, X., Jeong, C. -H., Godri, K. J., Sabaliauskas, K., and Slowik, J. G.: Mass absorption cross-section of ambient black carbon aerosol in relation to chemical age, Aerosol Sci. Tech., 43, 522–532, 2009.

Köylü, Ü. O., Xing, Y., and Rosner, D. E.: Fractal morphology analysis of combustion-generated aggregates using angular light scattering and electron microscope images, Langmuir, 11, 4848–4854, 1995.

Lack, D. A. and Cappa, C. D.: Impact of brown and clear carbon on light absorption enhancement, single scatter albedo and absorption wavelength dependence of black carbon, Atmos. Chem. Phys., 10, 4207–4220, doi:10.5194/acp-10-4207-2010, 2010.

Maricq, M. M. and Ning, X.: The effective density and fractal dimension of soot particles from premixed flames and motor vehicle exhaust, J. Aerosol Sci., 35, 1251–1274, 2004.

McMurry, P. H., Wang, X., Park, K., and Ehara, K.: The relationship between mass and mobility for atmospheric particles: A new technique for measuring particle density, Aerosol Sci. Tech., 36, 227–238, 2002.

Metcalf, A. R., Loza, C. L., Coggon, M. M., Craven, J. S., Jonsson, H. H., Flagan, R. C., and Seinfeld, J. H.: Secondary Organic Aerosol Coating Formation and Evaporation: Chamber Studies Using Black Carbon Seed Aerosol and the Single-Particle Soot Photometer, Aerosol Sci. Tech., 47, 326–347, 2013.

Moffet, R. C. and Prather, K. A.: In-situ measurements of the mixing state and optical properties of soot with implications for radiative forcing estimates, P. Natl. Acad. Sci. USA, 106, 11872–11877, 2009.

Moteki, N. and Kondo, Y.: Dependence of laser-induced incandescence on physical properties of black carbon aerosols: measurements and theoretical interpretation, Aerosol Sci. Tech., 44, 663–675, 2010.

Pagels, J., Khalizov, A. F., McMurry, P. H., and Zhang, R. Y.: Processing of Soot by Controlled Sulphuric Acid and Water Condensation Mass and Mobility Relationship, Aerosol Sci. Tech., 43, 629–640, 2009.

Park, K., Cao, F., Kittelson, D. B., and McMurry, P. H.: Relationship between particle mass and mobility for diesel exhaust particles, Environ. Sci. Technol., 37, 577–583, 2003.

Petzold, A., Ogren, J. A., Fiebig, M., Laj, P., Li, S.-M., Baltensperger, U., Holzer-Popp, T., Kinne, S., Pappalardo, G., Sugimoto, N., Wehrli, C., Wiedensohler, A., and Zhang, X.-Y.: Recommendations for reporting "black carbon" measurements, Atmos. Chem. Phys., 13, 8365–8379, doi:10.5194/acp-13-8365-2013, 2013.

Philippin, S., Wiedensohler , A., and Stratmann, F.: Measurements of non-volatile fractions of pollution aerosols with an eight-tube volatility tandem differential mobility analyzer (VTDMA-8), Aerosol Sci., 35, 185–203, 2004.

Qiu, C., Khalizov, A. F., and Zhang, R.: Soot aging from OH-initiated oxidation of toluene, Environ. Sci. Technol., 46, 9464–9472, 2012.

Radney, J. G., You, R., Ma, X., Conny, J., Hodges, J. T., Zachariah, M. R., Hodges, J. T., and Zangmeister, C. D.: Dependence of soot optical properties on particle morphology: measurements and model comparisons, Environ. Sci. Technol., 48, 3169–3176, 2014.

Rissler, J., Messing, M. E., Malik, A. I., Nilsson, P. T., Nordin, E. Z., Bohgard, M., Sanati, M., and Pagels, J. H.: Effective Density Characterization of Soot Agglomerates from Various Sources and Comparison to Aggregation Theory, Aerosol Sci. Tech., 47, 792–805, 2013.

Rissler J., Nordin, E. Z., Eriksson, A. C., Nilsson, P. T., Frosch, M., Sporre, M. K., Wierzbicka, A., Svenningsson, B., Löndahl, J., Messing, M. E., Sjogren, S., Hemmingsen, J. G., Loft, S., Pagels, J. P., and Swietlicki, E.: Effective density and mixing state of aerosol particles in a near-traffic urban environment, Environ. Sci. Technol., 48, 6300–6308, 2014.

Scarnato, B. V., Vahidinia, S., Richard, D. T., and Kirchstetter, T. W.: Effects of internal mixing and aggregate morphology on optical properties of black carbon using a discrete dipole approximation model, Atmos. Chem. Phys., 13, 5089–5101, doi:10.5194/acp-13-5089-2013, 2013.

Schwarz, J. P., Gao, R. S., Fahey, D. W., Thomson, D. S., Watts, L. A., Wilson, J. C., Reeves, J. M., Darbeheshti, M., Baumgardner, D. G., Kok, G. L., Chung, S. H., Schulz, M., Hendricks, J., Lauer, A., Kärcher, B., Slowik, J. G., Rosenlof, K. H., Thompson, T. L., Langford, A. O., Loewenstein, M., and Aikin, K. C.: Single-Particle Measurements of Midlatitude Black Carbon and Light-Scattering Aerosols from the Boundary Layer to

the Lower Stratosphere, J. Geophys. Res.-Atmos., 111, D16207, doi:10.1029/2006JD007076, 2006.

Sgro, L. A., Basile, G., Barone, A. C., D'Anna, A., Minutolo, P., Borghese, A., and D'Alessio, A.: Detection of combustion formed nanoparticles, Chemosphere, 51, 1079–1090, 2003.

Slowik, J. G., Stainken, K., Davidovits, P., Williams, L. R., Jayne, J. T., Kolb, C. E., Worsnop, D. R., Rudich, Y., DeCarlo, P. F., and Jimenez, J. L.: Particle morphology and density characterization by combined mobility and aerodynamic diameter measurements. Part 2: Application to combustion-generated soot aerosols as a function of fuel equivalence ratio, Aerosol Sci. Tech., 38, 1206–1222, 2004.

Slowik, J. G., Cross, E. S., Han, J.-H., Kolucki, J., Davidovits, P., Williams, L. R., Onasch, T. B., Jayne, J. T., Kolb, C. E., and Worsnop, D. R.: Measurements of Morphology Changes of Fractal Soot Particles using Coating and Denuding Experiments: Implications for Optical Absorption and Atmospheric Lifetime, Aerosol Sci. Tech., 41, 734–750, 2007.

Tuch, T. M., Haudek, A., Müller, T., Nowak, A., Wex, H., and Wiedensohler, A.: Design and performance of an automatic regenerating adsorption aerosol dryer for continuous operation at monitoring sites, Atmos. Meas. Tech., 2, 417–422, doi:10.5194/amt-2-417-2009, 2009.

Wehner, B., Berghof, M., Cheng, Y. F., Achtert, P., Birmili, W., Nowak, A., Wiedensohler, A., Garland, R. M., Pöschl, U., Hu, M., and Zhu, T.: Mixing state of nonvolatile aerosol particle fractions and comparison with light absorption in the polluted Beijing region, J. Geophys. Res., 114, D010923, doi:10.1029/2008JD010923, 2009.

Xue, H., Khalizov, A. F., Wang, L., Zheng, J., and Zhang, R.: Effects of dicarboxylic acid coating on the optical properties of soot, Phys. Chem. Chem. Phys., 11, 7869–7875, 2009a.

Xue, H. X., Khalizov, A. F., Wang, L., Zheng, J., and Zhang, R. Y.: Effects of Coating of Dicarboxylic Acids on the Mass-Mobility Relationship of Soot Particles, Environ. Sci. Technol., 43, 2787–2792, 2009b.

Zhang, R., Khalizov, A. F., Pagels, J., Zhang, D., Xue, H., and McMurry, P. H.: Variability in morphology, hygroscopicity, and optical properties of soot aerosols during atmospheric processing, P. Natl. Acad. Sci. USA, 105, 10291–10296, 2008.